Oxytocin enhancement of CA1 spike transmission by modulation of fast-spiking interneurons

Scott F. Owen[1], **Sebnem N. Tuncdemir**[2], **Patrick L. Bader**[2], **Natasha N. Tirko**[2], **Gord Fishell**[2], and **Richard W. Tsien**[2]

[1]Department of Molecular and Cellular Physiology, Stanford University School of Medicine, Stanford, California, USA 94305

[2]NYU Neuroscience Institute, New York University, New York NY 10022

Keywords

Summary

Neuromodulatory control by oxytocin is essential to a wide range of social[1,2], parental[3] and stress-related behaviors[4]. Autism spectrum disorders (ASD) are associated with deficiencies in oxytocin levels[5] and with genetic alterations of the oxytocin receptor (OXTR)[6]. Thirty years ago, Muhlethaler *et al.*[7] found that oxytocin increases the firing of inhibitory hippocampal neurons, but it remains unclear how elevated inhibition could account for the ability of oxytocin to improve information processing in the brain. Here, we describe a simple yet powerful mechanism by which oxytocin enhances cortical information transfer[8] while simultaneously lowering background activity, thus greatly improving signal-to-noise. Increased fast-spiking interneuron (FSI) activity not only suppresses spontaneous pyramidal cell firing, but also enhances the fidelity of spike transmission and sharpens spike timing. Use-dependent depression at the FSI-pyramidal cell synapse is both necessary and sufficient for the enhanced spike throughput. Notably, we show the generality of this novel circuit mechanism by activation of FSIs with cholecystokinin, or with channelrhodopsin-2. This provides insight into how a diffusely delivered neuromodulator can improve the performance of neural circuitry that requires synapse specificity and millisecond precision.

Corresponding Author: Dr. Richard W. Tsien, NYU Neuroscience Institute, New York University, East River Science Park, Alexandria Center, 450 East 29th St, 9th Floor, New York, NY 10016, 650-799-1019, richard.tsien@nyumc.org.

Results

The CA1 region of hippocampus receives potent excitatory input from neighboring area CA3 through the Schaffer Collateral (SC) pathway. Activation of SC axons evokes a monosynaptic excitatory post-synaptic potential (EPSP) onto CA1 pyramidal cells, as well as exciting a variety of CA1 interneurons. These interneurons then deliver a millisecond-delayed inhibitory postsynaptic potential (IPSP), termed feed-forward inhibition. Thus, both the stimulation threshold and the timing of spikes evoked in CA1 pyramidal cells by SC activation are dictated by a finely tuned balance of monosynaptic excitatory and disynaptic inhibitory inputs[8,9].

In agreement with previous results[8], we found that stimulation of the SC pathway in acute rat hippocampal slices evoked spikes with a short latency and moderate jitter (Fig 1a). Strikingly, bath application of TGOT (Thr[4],Gly[7]-Oxytocin, 200 nM), a specific agonist for oxytocin receptors, dramatically increased the probability of evoking a spike in the postsynaptic neuron from 0.50 to 0.82, while simultaneously suppressing the spontaneous activity of CA1 pyramidal cells by 57% from 1.4 Hz to 0.6 Hz (Fig 1a–d). The combination of increased evoked spike probability (signal) and reduced spontaneous activity (noise) resulted in an enhanced signal-to-noise. TGOT also reduced the latency and increased the temporal precision of evoked spikes (Fig 1e,f).

In agreement with previous work[7,10], TGOT increased the rate and amplitude of spontaneous inhibitory postsynaptic currents (IPSCs) onto CA1 pyramidal cells (Fig 1g, S1). Blockade by 10 μM bicuculline or by 100 nM tetrodotoxin indicated that these events were mediated by $GABA_A$ receptors and likely required an increase in interneuron firing rather than a change in spontaneous presynaptic release. The specific oxytocin receptor antagonist OTA (($d(CH_2)_5$[1],Tyr(Me)[2],Thr[4],Orn[8],des-Gly-NH_2[9])-Vasotocin, 1 μM) blocked the TGOT-induced effects, suggesting that these actions were solely mediated by the oxytocin receptor[10]. The TGOT-induced increase in spontaneous IPSCs was also abolished by the potent P/Q-type calcium channel blocker ω-Agatoxin IVA, but unaffected by the N-type calcium channel antagonist ω-Conotoxin GVIA, suggesting that these events primarily arise from FSIs with little contribution from RS interneurons (Fig 1g, S1)[11,12].

To test more directly whether TGOT precisely targeted FS interneuron subtypes, we used whole cell recordings in CA1 strata oriens and pyramidale, stratum radiatum interneurons being unresponsive to TGOT[10] and lacking OXTR expression[13]. We found a clear distinction: FSIs were responsive to TGOT, whereas RS interneurons were not (Fig 2a). FSIs displayed robust responses upon application of 20 and 200 nM TGOT (Fig S2a–c), the latter producing a near-saturated effect. Dividing the increase in IPSCs onto pyramidal cells (27.3 Hz, Fig 1g) by the increase in FSI firing rate (8.8 Hz per FSI, Fig 2a), we calculate that on average each pyramidal cell receives input from at least ~3.1 TGOT-responsive FSIs in our slices.

To clarify mechanisms by which TGOT depolarizes FSIs, we voltage clamped FS perisomatic-targeting (basket and axo-axonic) and RS basket cells at −65 mV. TGOT induced a large inward current in FSIs (Fig 2b, S2g), but as expected had no effect on the RS

cells (data not shown). TGOT also increased the rate of spontaneous IPSCs onto the FSI (Fig S2d–f), as predicted from the FSI-FSI connectivity that may serve to regulate the distribution and extent of inhibition.

To test whether the TGOT-induced inward current arises from G-protein signaling within the FSI itself, we replaced the GTP in the intracellular recording solution with 1 mM GTPγS, a non-hydrolysable GTP analog that renders G-proteins constitutively active. The GTPγS-induced current largely occluded the TGOT-induced current (Fig 2b, S2g), verifying that the TGOT effects involve G-protein signaling within the recorded neuron. The amplitude and kinetics of the TGOT-induced current were unaffected by intracellular BAPTA, indicating that the intracellular signaling mechanism is likely not Ca^{2+}-dependent[14]. In voltage ramp recordings from FSIs, the TGOT-induced current reversed at −3.1±3.4 mV (Fig 2c, S2h), suggesting that the currents were generated by a non-selective cation channel. Partial replacement of external sodium by NMDG (50 mM) shifted the reversal potential to more negative values (−13.8±3.7 mV, P<0.05 unpaired two-tailed t-test, data not shown), pointing to Na^+ as the predominant charge carrier of the TGOT-induced inward current.

To investigate the mechanisms of the enhanced fidelity of spike transmission, we obtained whole cell current clamp recordings from CA1 pyramidal cells and elicited spikes synaptically or by current injection on interleaved trials (Fig 2d,e, S3, S4a). TGOT increased the fidelity of synaptically evoked spikes in whole cell mode, paralleling its effect in cell-attached recordings (Fig 1), but reduced the probability of evoking spikes by whole cell current injection. This apparent reduction in pyramidal cell excitability was coupled to a hyperpolarization of the cell membrane (Fig S4b). As TGOT had no effect on the holding current or membrane resistance in voltage clamp recordings of pyramidal neurons in the presence of bicuculline (Fig S4c), we concluded that the reduction in spontaneous activity and excitability was wholly attributable to enhanced inhibitory tone. This increase in inhibitory tone, however, made the enhanced EPSP-spike coupling all the more surprising.

We hypothesized that the enhanced EPSP-spike coupling might arise from a shift in the synaptic excitatory-inhibitory balance. Indeed, the disynaptic IPSP was reduced by TGOT (Fig S4g,h), and bicuculline abolished the TGOT-induced increase in evoked spike probability in cell-attached recordings (Fig 2f). To most rigorously isolate inhibitory inputs, we stimulated the Schaffer Collaterals while holding the cell at 0 mV under voltage clamp, and found that the evoked disynaptic IPSC was reduced by TGOT (Fig 2g,h). In contrast, the evoked excitatory postsynaptic current (EPSC), isolated at −65 mV in the presence of bicuculline, was unaffected. This selective reduction of the evoked IPSC while sparing the EPSC, shifts the excitatory-inhibitory (E-I) balance and could account for the increase in evoked spike probability. This reduction in feed-forward inhibition could arise from either a reduction in excitatory to inhibitory (E→I) transmission, causing fewer interneurons to be activated, or a reduction in inhibitory to excitatory (I→E) transmission, causing each interneuron to be less effective. We recorded from FSIs while stimulating the SC pathway but found no effect of TGOT on E→I transmission (Fig S4i,j). In contrast, stimulating the stratum pyramidale while blocking excitatory transmission with NBQX and AP5 revealed a TGOT-induced suppression of I→E transmission onto pyramidal cells (Fig S4k,l).

Using paired whole cell recordings, we investigated how TGOT reduces the evoked IPSC at the I→E synapse. TGOT increased the spontaneous firing of presynaptic FSIs and also diminished the FSI-pyramidal cell unitary IPSC, without affecting RS interneurons (Fig 3a,b). When the TGOT-induced depolarization of the presynaptic FSI was countered with a hyperpolarizing bias current, however, the spontaneous firing in the presynaptic cell ceased and the unitary evoked IPSC was maintained at its pre-TGOT amplitude. This rescue suggests that TGOT induces a use-dependent depression of the IPSC[15,16], and that the increase in spontaneous FSI firing is *necessary* for the reduction in the evoked feed-forward IPSC.

To test whether the TGOT-induced increase in the FSI firing rate was *sufficient* to account for the observed synaptic depression, we drove 10 s trains of action potentials in the absence of TGOT (Fig 3c). The frequency dependence of the residual IPSC following a 10 s train in control ACSF (Fig 3d, colored diamonds) matched closely with that of the residual IPSC in TGOT (Fig 3d, black symbols). Thus, the TGOT-mediated increase in FSI spontaneous firing is not only *necessary* (Fig 3a,b) but also *sufficient* (Fig 3c,d) to account for the observed decrease in evoked IPSC amplitude (Fig 2g,h), and enhancement of EPSP-spike coupling (Fig 1). Recovery of the IPSC was nearly complete by 4.5 s following the 50 Hz train, consistent with a rapid switching of the FS synapses between baseline and depressed states[16] (Fig 3e). We also observed a modest, frequency-dependent increase in the spike width over the 10 s trains (Fig S5) that would be expected, if anything, to increase presynaptic release, contrary to the use-dependent depression that was observed.

The specificity of TGOT for FSIs suggested that this mechanism may be a general property of this network, and that any peptide, network state, or signal that increases the spontaneous activity of FSIs will also increase the fidelity of spike transmission. We tested this hypothesis using two independent approaches, first stimulating FSIs with the peptide cholecystokinin (CCK), and second targeting this population with the light-activated ion channel channelrhodopsin-2 (ChR2).

CCK activates FS basket cells[11], transiently increasing their firing rate in a manner reminiscent of TGOT. In close agreement with our TGOT results, CCK enhanced inhibitory tone and suppressed the evoked feed-forward IPSC without affecting the evoked EPSC (Fig 4a,b, S6). In cell-attached recordings, CCK increased the probability of evoking spikes in CA1 pyramidal cells by SC stimulation, while simultaneously suppressing the spontaneous firing of these cells (Fig 4c,d). Furthermore, both the latency and the jitter of the evoked spikes were reduced by CCK (Fig S6f), just as they were with TGOT (Fig 1f).

We then used ChR2 to selectively activate FSIs in acute hippocampal slices from PV-cre BAC transgenic mice. Immunostaining confirmed that the ChR2 was efficiently targeted to the parvalbumin-expressing (PV+) FSIs (Fig S7). Optogenetic activation of FSIs induced IPSCs in CA1 pyramidal cells that showed a strong synaptic depression (Fig 4e), consistent with our paired recording data (Fig 3), and with previous reports[15,16]. In agreement with our TGOT and CCK results, driving FSIs with a brief train of blue light pulses preceding an electrical stimulus to the SC pathway modestly increased the probability of eliciting a spike in a postsynaptic pyramidal cell, relative to interleaved control trials in which the blue light

was omitted (Fig S8a). Examination of the spike latency and jitter, however, revealed a high probability that monosynaptic inhibition contaminated a subset of these recordings. When the recordings with the shortest latency and lowest jitter were excluded (Fig S8d–f, see methods), the remaining neurons all exhibited a pronounced increase in evoked spike probability following ChR2 stimulation (Fig 4f,g). Taken together, three interventions, TGOT, CCK and ChR2, therefore all converge on a single surprising conclusion: that activation of FSIs enhances the fidelity of spike transmission in the hippocampus. TGOT also increased the evoked population spike amplitude in the presence of kainate-induced gamma rhythms (Fig S9), thus confirming that the TGOT-induced enhancement in EPSP-spike coupling is robust under more *in vivo*-like conditions.

We constructed a minimal computational model to investigate the mechanisms linking FSI activation to the evoked spike probability, latency and jitter. We mimicked the enhanced FSI activity by increasing the rate and amplitude of spontaneous IPSCs. The synaptic depression at the FSI-pyramidal synapse was simulated by reducing the evoked IPSC to 60% of its basal value. In agreement with our experimental results, these changes reduced the simulated evoked IPSP, increased the simulated evoked spike probability, and sharpened the evoked spike timing (Fig S10).

We then asked why a decrease in feed-forward inhibition shrinks evoked spike latency and jitter, in apparent conflict with the idea that feed-forward inhibition enforces sharp spike timing[8,9]. Resolution is achieved by considering how the EPSC and IPSC conductances (g_{EPSC} and g_{IPSC}) regulate membrane voltage near the spike-firing threshold. A reduction in g_{IPSC} allows an unaltered g_{EPSC} to push the membrane potential up to the spike firing threshold more reliably and more quickly and precisely (Fig 4h,i). In contrast, if g_{EPSC} is reduced to nearly the same degree as g_{IPSC} in order to clamp the likelihood of spike firing[8], the latency and jitter are increased.

Finally, we probed the functional consequences of the strikingly incomplete depression of the FS synapses (Fig 3c) and the effects of varying the latency between the onset of g_{EPSC} and g_{IPSC}. Fidelity of spike transmission (defined as the fraction of sweeps containing precisely one postsynaptic spike) is maximal when IPSCs are depressed by approximately 40% (Fig 4j), the value we observed experimentally in response to either TGOT or CCK application (Fig 2g,h, 4a,b). Likewise, a residual IPSC of 50–60% was optimal in considerations of global spike jitter (Fig S10h). Thus, the empirically observed TGOT response in FSIs seems well suited in multiple respects to the efficient retuning of overall circuit performance.

Discussion

Our experiments reveal a generalized mechanism through which oxytocin improves the fidelity and temporal precision of information transfer through brain networks. Oxytocin enhanced circuit performance in three ways: increasing throughput of output spikes, sharpening submillisecond spike timing, and suppressing background firing. Each of these improvements in circuit signal-to-noise could be traced to the action of oxytocin on FSIs and

reproduced through quantitative simulations, as well as through other interventions that specifically activate FSIs.

The rapid onset and recovery of FSI use-dependent synaptic depression is well suited to shift circuit dynamics rapidly yet stably in response to oxytocin, whether delivered quickly and focally, as in synaptic release[4], or presented diffusely at low doses, as in volume transmission. The partial depression of FSI synapses (residual, ~35%) and the sparing of RS interneurons ensures that modulation by oxytocin avoids the dangers associated with a complete loss of inhibition such as dramatically impaired spike timing precision[8] (Fig S10, S11) and epileptogenesis.

Our experiments provide a circuit mechanism linking three disparate aspects of ASD[17]. *Oxytocin signaling* has been implicated in ASD by genetic analysis and pharmacological studies[18,19]. *PV-positive FSIs* are important in autism etiology[20], presumably due to their role in excitation-inhibition balance and neuronal oscillations, both of which are likely impaired in ASD. *Deficiencies in signal-to-noise*, observed as unreliable cortical evoked potentials in ASD[21], offer a valuable endophenotype, but have not yet been linked to a circuit defect or a therapeutic strategy. Our finding that FSIs are direct targets of oxytocin[18,19] and can potently modulate circuit signal-to-noise, shows these cells may be uniquely poised to counteract deficits in rapid information processing in psychiatric disorders[21]. In healthy individuals, oxytocin signaling through FSIs may provide a salience cue, capable of transiently enhancing cognitive performance[1,3,22]. Indeed, increasing PV+ interneuron activity was sufficient to recover hippocampal-dependent behavioral deficits in a mouse model of Alzheimer's Disease[23]. There may be parallels in the visual cortex as well, where optogenetic activation of PV+ interneurons operates like a salience cue and sharpens orientation tuning[24].

What is the functional logic for oxytocin selectively targeting FSIs amidst the wide variety of interneuron types? One rationale is that the FSIs engaged by oxytocin are physiologically and functionally distinct from RS interneurons, which themselves are regulated by endocannabinoids[25]. Thus, by targeting select interneuron populations, neuromodulators are able to regulate different forms of inhibition, with oxytocin affecting feed-forward inhibition and endocannabinoids tuning feed-back inhibition.

Another modulator, noradrenaline (NA) enhances circuit signal-to-noise in slice and *in vivo* through a variety of mechanisms across multiple brain regions including the hippocampus[26,27] and auditory system[28]. In auditory brainstem, Kuo and Trussell elegantly described how NA suppresses cartwheel inhibitory neuron spiking, relieving their output synapses from tonic depression[28]. Although their mechanism differs from ours in direction of change and functional outcome, an emergent general principle is that modulation of inhibitory neuron tonic firing and variation in use-dependent synaptic depression can regulate signal-to-noise. In the hippocampus, Madison, Nicoll and colleagues delineated several monoamine responses across excitatory and inhibitory neurons that enhance circuit signal-to-noise[26,29,30]. Although oxytocin and NA both enhance signal-to-noise of CA1 pyramidal neurons, the widespread effects of NA contrast sharply with the exquisitely focused mechanism we uncovered. Oxytocin accomplishes both the enhanced fidelity of

spike transmission and the suppression of background activity by selectively targeting a single locus: FSI activity. Furthermore, FSI synaptic depression in hippocampal CA1 (Fig 4) is representative of that in dentate gyrus[16], cortex[15], and elsewhere, suggesting similar modulation of signal-to-noise by FSI activity may be essential in many brain regions.

Methods

Slice preparation

Rat hippocampal slices (350 μm thick) were prepared using a Leica VT 1000S vibratome from p21-p28 Sprague-Dawley rats of either sex in ice-cold sucrose slicing solution containing (in mM) 206 Sucrose, 11 D-Glucose, 2.5 KCl, 1 NaH_2PO_4, 10 $MgCl_2$, 2 $CaCl_2$ and 26 $NaHCO_3$. Rats were anaesthetized with isoflurane inhalation before decapitation and dissecting out of the hippocampus. Mouse transverse hippocampal slices (300μm) were prepared using a Vibratome 1000 plus (Vibratome, St. Louis, MO). Mice were deeply anaesthetized with intraperitoneal injection of pentobarbital (100 mg/kg body weight) and then transcardially perfused with ~30 ml ice-cold sucrose-ACSF solution containing (in mM) 252 sucrose, 24 $NaHCO_3$, 1.25 NaH_2PO_4, 3 KCl, 2 $MgSO_4$, 10 D-Glucose and 0.5 $CaCl_2$. All slices from rats and mice were allowed to recover submerged in artificial cerebro-spinal fluid (ACSF) for 1 hr at 34°C, and then maintained at room temperature until recording. For recordings from rat tissue, ACSF contained (in mM) 122 NaCl, 3 KCl, 10 D-Glucose, 1.25 NaH_2PO_4, 2 $CaCl_2$, 1.3 $MgCl_2$, 26 $NaHCO_3$, 3 Na-Pyruvate, 2 Na-Ascorbate and 5 L-Glutamine. For mouse recordings, ACSF contained (mM) 124 NaCl, 26 $NaHCO_3$, 2.5 KCl, 1.25 NaH_2PO_4, 2 $CaCl_2$, 2 $MgSO_4$, 5 L-Glutamine, and 10 D-Glucose. All slice preparation and recording solutions were oxygenated with carbogen gas (95% O_2/5% CO_2, pH 7.4).

Electrophysiological recordings

Recordings were performed in a submerged chamber at 32–34°C with constant bath perfusion of ACSF at ~5 mL/minute for rats, ~2 mL/minute for mice. Slices were allowed 15–45 min to equilibrate before recording. Because the $GABA_B$ blocker CGP52432 (2 μM) did not affect the TGOT enhancement of evoked spike probability, recordings were pooled from control ACSF (N=7 cells) and CGP52432 (N=8 cells) conditions to measure spike probability, suppression of spontaneous firing, and evoked spike timing (Fig 1). For cell-attached measurement of TGOT influence on spontaneous activity, results were pooled from recordings in control ACSF (N=15 cells) and in the presence of CGP52432 at 2 μM (N=8 cells). To prevent ictal activity, the CA3 region of each slice was removed before recordings in bicuculline. Recordings were made using glass pipettes with a tip resistance of 2–4 MΩ. For cell-attached recordings, pipettes were filled with ACSF and the amplifier was set in voltage clamp mode. Slices were visualized with an upright microscope (Zeiss Axioskop 2 FS plus) using infrared differential interference contrast (IR-DIC) optics. Data were recorded with a MultiClamp 700B amplifier (Axon Instruments, Union City, CA), filtered at 10 kHz using a Bessel filter and digitized at 20 kHz with a Digidata 1322A analog-digital interface (Axon Instruments). For whole cell recordings, experiments were discarded if the series resistance changed significantly or reached 20 MΩ. Spontaneous IPSCs onto pyramidal cells were detected in voltage clamp using a 50 mM Cl⁻ internal solution

containing (in mM) 70 CsMeSO$_3$, 35 CsCl, 15 TEA-Cl, 1 MgCl$_2$, 0.2 CaCl$_2$, 10 HEPES, 0.3 EGTA, 10 Tris-Phosphocreatine, 4 Mg-ATP, and 0.3 Na-GTP. For evoked IPSC and EPSC recordings, the internal solution contained (in mM) 130 CsMeSO$_3$, 8 CsCl, 1 MgCl$_2$, 10 HEPES, 0.3 EGTA, 10 Tris-Phosphocreatine, 4 Mg-ATP, and 0.3 Na-GTP. Bicuculline (10 μM), TTX (100 nM) and OTA (1 μM) were delivered as indicated in the bathing solution throughout the recording (Fig 1, S1). Calcium channel blockers ω-agatoxin IVA at 0.5 μM (AgaIVA) or ω-conotoxin GVIA at 1 μM (GVIA) were delivered by pre-treating the slice for 30 min in an interface chamber before recording in control ACSF. AgaIVA and GVIA recordings were performed in separate slices from the same experimental animal.

Synaptic events were evoked using a tungsten bipolar stimulating electrode placed in the Schaffer Collateral excitatory afferents from area CA3 to deliver stimuli 100 μs in duration. With the exception of Figure S4k,l, the stimulating electrode was placed far from the recorded cell (~400 μm to ~800 μm) to minimize monosynaptically evoked IPSCs. In Figure S4k,l, monosynaptic IPSCs were evoked using sub-maximal stimulation by placing the stimulating electrode in the pyramidal cell layer close to the recorded cell (~100 μM), and including 10 μM NBQX and 50 μM AP5 in the bath to block excitatory transmission. For evoked IPSP measurement, data were pooled from evoked spike successes and failures and from recordings in the presence (N=5 cells) or the absence (N=1 cell) of the GABA$_B$ antagonist CGP52432 (2 μM). Evoked disynaptic feed-forward IPSCs (Fig 2g,h; Fig 4a,b) were recorded as outward currents at a holding potential of 0 mV in control ACSF. Evoked EPSCs were isolated by including 10 μM bicuculline in the bath and holding the cell at −65 mV. Two out of 14 recordings in Figs 4c,d and S6e,f were performed in the continuous presence of AM-251 (2 μM) to confirm the persistence of the CCK-induced enhancement of EPSP-spike coupling even when endocannabinoid signaling was blocked.

For current clamp recordings, and all interneuron recordings except for the voltage ramp experiments, the intracellular solution contained (in mM) 130 K-Gluconate, 1 MgCl$_2$, 10 HEPES, 0.3 EGTA, 10 Tris-Phosphocreatine, 4 Mg-ATP, and 0.3 Na-GTP. For interneuron recordings this solution was supplemented with 0.1% biocytin. GTP was omitted in experiments featuring GTPγS. For voltage clamp recordings of TGOT-induced currents in FSIs, traces were divided into 10 s segments, with the mean value of each segment plotted as a function of time to exclude synaptic events. See Fig S2d for exemplar raw trace. All recordings were baseline-subtracted to adjust for the leak current measured during the first 2 min before the onset of the GTPγS-induced current. Traces were time-aligned to the wash-in of TGOT (red bar). For one cell in the GTPγS data set in which baseline recording period was 10 min rather than 15 min, the pre-TGOT period was aligned to the start of the other recordings, and the remainder of the trace starting with TGOT wash-in was aligned to the TGOT wash-in of the other traces.

FSI Voltage Ramp Recordings

For voltage ramp recordings, the internal solution contained (in mM) 50 K-Gluconate, 70 CsMeSO$_3$, 10 TEA-Cl, 1 MgCl$_2$, 10 HEPES, 0.3 EGTA, 10 Tris-Phosphocreatine, 4 Mg-ATP, and 0.3 Na-GTP. The pipette reference potential was set to zero and a junction potential of −15.1 mV (calculated using pClamp) was corrected *post hoc*. An additional,

empirically measured correction factor of 3.3 mV was applied to correct for a change in the junction potential introduced by partial replacement of sodium with NMDG in the voltage ramp ACSF. Apart from the voltage ramp recordings, other membrane potentials reported are not corrected for liquid junction potentials. After obtaining a whole cell recording from a putative interneuron, the fast-spiking phenotype was verified as described below. The amplifier was then switched to voltage clamp mode and the bath solution was substituted for Voltage Ramp ACSF containing (in mM) 112 NaCl, 10 D-Glucose, 3 KCl, 1.25 NaH_2PO_4, 10 TEA-Cl, 1.3 $MgCl_2$, 2 $CaCl_2$, 26 $NaHCO_3$, 5 4-Aminopyridine, 0.1 $CdCl_2$ and 0.001 TTX. Voltage ramps ~1 s in duration between −91 and +29 mV were applied once every 10 s until the current at each potential reached a steady state for >2 min, at which point TGOT was applied. In 3 out of 13 recordings the voltage ramp-activated current (1) became more negative at all potentials shortly after TGOT application, and (2) failed to return to baseline after washout of the drug. It was assumed that this global shift was caused by a change in the space clamp or access resistance and these recordings were excluded from further analysis.

Drugs and reagents

All salts and buffers for intracellular and extracellular solutions, as well as ATP, GTP, GTPγS, phosphocreatine and biocytin were purchased from Sigma (St. Louis, MO). TGOT ((Thr^4,Gly^7)-Oxytocin), OTA ((d(CH_2)$_5$^{1},Tyr(Me)^2,Thr^4,Orn^8, des-Gly-NH$_2$^{9})-Vasotocin) and CCK (cholecystokinin octapeptide) peptides were purchased from Bachem (Torrance, CA), dissolved at 1 mM in ddH_2O and stored at −20°C until use within 6 months of purchase. Bicuculline, TTX, NBQX, and D-AP5 were purchased from Ascent Scientific (Princeton, NJ). ω-conotoxin GVIA and ω-agatoxin IVA were purchased from Peptides International (Louisville, KY). Stock solutions were prepared and stored according to manufacturer specifications.

Interneuron labeling and classification

Physiological classification of interneuron subtypes was based on established criteria[11,25,31]. Fast-spiking cells were defined as those including (1) peak firing rates >200 Hz with little firing rate accommodation, (2) characteristic FS action potential waveform, and (3) minimal hyperpolarization-induced sag current due to I_h. Following interneuron recordings, slices were transferred to a fixative solution containing 4% paraformaldehyde, 0.2 % picric acid and 1× phosphate buffered saline for 24–72 h before being stained with 3,3'-diaminobenzidine tetrahydrochloride (0.015%) using a standard ABC kit (Vector). Neuronal cell types were identified based on morphology of axonal and dendritic arbors and electrophysiological properties of the cell. The FS perisomatic-targeting set includes both basket cells (shown), and axo-axonic cells (not shown). Because of technical challenges of discriminating FS basket and axo-axonic cells unequivocally, both cell types were pooled into a single group of FS perisomatic-targeting cells. When analyzed separately, both putative types were equivalently responsive to TGOT.

Analysis of cell-attached and intracellular recording data

Analysis of spikes, evoked synaptic currents, and synaptic potentials were performed offline using custom written routines in MATLAB (Mathworks). Spontaneous IPSCs were detected using a modified version of the detectPSPs script by Phil Larimer (http://

www.mathworks.com/matlabcentral/fileexchange). Spike jitter histograms were calculated by subtracting the latency of each spike from the average latency of spikes evoked in that cell. The average latency and jitter were calculated separately for control and TGOT/CCK conditions in each cell. To measure the spike width, raw data was oversampled to 133 kHz using the MATLAB spline function. Time course of spontaneous activity in pyramidal cell attached recordings was calculated by averaging over all cells and smoothing in time with a boxcar filter (width=7 sweeps).

Optical stimulation of channelrhodopsin-2

Photostimuli were produced by three Luxeon Rebel LEDs (470 nm, Philips Lumileds, San Jose, CA) driven by a custom-built controller. The LEDs were placed below the recording chamber for full slice illumination once stable recording conditions were reached. Light pulses were 5 ms in duration with a power of approximately 0.5 mW/mm^2. ChR2-evoked IPSCs were recorded from CA1 pyramidal neurons (n=10 cells, N=4 animals). Six of these neurons were recorded in the same region of the same slice as neurons recorded in the cell-attached data set.

Data analysis for cell-attached recordings involving blue light stimulation

In the full data set, blue light stimulation increased the spike probability in 13 of 16 neurons (Fig S8a, 12% increase in spike probability including all neurons, P<0.05, two-tailed *t*-test). In recordings from rat neurons the average increase in spike firing probability with TGOT or CCK was not correlated with spike latency, whereas in the mouse data we found a strong correlation between control spike latency and the ChR2-induced increase in spike probability (Fig S8d,e). In the mouse data set, the shortest latency spikes showed the weakest increase in spike firing probability. Plotting the latency against the jitter of spikes elicited under control conditions, we found a clear separation between two groups of cells, in which evoked spikes from one set of cells occurred with very short latency and little jitter and spikes from another set of cells occurred at longer latency and with more jitter (Fig S8f).

Because of the smaller size of the mouse brain, we found our slice angle to be less reliably transverse than in the rat preparation. As a result, the stimulating and recording electrodes were placed closer to one another in the mouse slice in order for the stimulating electrode to recruit a sufficient number of excitatory Schaffer Collateral fibers to drive an action potential in the postsynaptic CA1 pyramidal cell. This change in recording configuration unfortunately increases the probability of directly activating inhibitory fibers with the stimulating electrode and generating a monosynaptic IPSC. A well-documented set of physiological parameters, including synaptic kinetics and cell excitability[25] ensure that the physiologically relevant disynaptic IPSC arises mostly from FSIs. The monosynaptically activated IPSC, however, will arise from a less targeted subset of neurons, and therefore be less susceptible to modulation by interventions that selectively target FSIs.

In the cell-attached recording configuration, it was impossible to determine directly the relative monosynaptic and disynaptic contributions to the feed-forward IPSC. The monosynaptic IPSC relies only on a single GABAergic synapse, however, whereas the disynaptic IPSC relies on three sequential steps: (1) a glutamatergic synapse onto the

interneuron, (2) the subsequent action potential in the interneuron, and finally (3) the GABAergic transmission onto the postsynaptic pyramidal cell. The monosynaptic IPSC will therefore occur with a shorter latency and less jitter than the disynaptically evoked IPSC. As a result, spikes in pyramidal cells in which the feed-forward IPSC is dominated by a monosynaptic component will be expected to occur with a shorter latency and less jitter than spikes in cells experiencing a more physiological disynaptic feed-forward IPSC. We therefore excluded the tightly clustered group of neurons with very short latency and low jitter spikes from the mouse data set (N=9 cells) and analyzed only the neurons in which spikes occurred with a longer latency and more jitter, consistent with disynaptic feed-forward inhibition (N=7 cells). All of these remaining cells demonstrated an increase in spike firing probability following blue light stimulation (7 out of 7 cells, 28% increase in spike probability; P<0.01 paired two-tailed t-test). In the complete data set (N = 16 cells) we observed a modest increase in spike latency following blue light stimulation of PV interneurons across all 16 neurons (Fig S8b,c). However, in the 5 out of 7 cells from the restricted data set that fired at least 5 spikes in both the control and blue light stimulation conditions, light activation of PV interneurons reduced the latency (Fig S8g, 10.35 ms in control, 10.07 ms following light stimulation; P = 0.73 paired two-tailed t-test) and jitter (Fig S8h, 16.58 ms^2 control; 11.78 ms^2 light stimulation; P = 0.23 paired two-tailed t-test) of spikes. Although this reduction in latency and jitter did not reach statistical significance, the trend is consistent with our TGOT and CCK results.

Immunohistochemistry

At the end of each ChR2 recording session, slices were fixed overnight with 4% paraformaldehyde (PFA)/phosphate buffered saline (PBS) solution and cryoprotected by immersion in 30% sucrose/PBS solution overnight at 4°C. Tissues were embedded in Tissue Tek, frozen on dry ice, and cryosectioned at 20 μm thickness. Sections for were processed using 1.5% normal goat serum (NGS) and 0.1% Triton X-100 in all procedures except washing steps, where only PBS was used. Sections were incubated in blocking solution for 1 hr, followed by incubation with the primary antibodies overnight at 4°C. Cryostat tissue sections were stained with the primary antibodies: mouse anti-Parvalbumin (1:1000, Sigma) and rabbit anti-DsRed (1:500, Chemicon). Secondary antibodies conjugated with Alexa fluoro dyes 488, 594 (Molecular Probes) raised from the same host used for blocking serum were applied for 1 hr at room temperature. Nuclear counterstaining was performed with 100 ng/ml 4,6-diamidino-2-phenylindole (DAPI) solution in PBS for 5 min. Fluorescent images were captured using a cooled-CCD camera (Princeton Scientific Instruments, NJ) using Metamorph software (Universal imaging, Downingtown, Pennsylvania).

Virus injection

Adeno-associated virus carrying ChR2 fused to the fluorescent marker mCherry AAV2/1.EF1.dflox.hChR2(H134R)-mCherry.WPRE.hGH, (University of Pennsylvania Gene Therapy Program Vector Core) was injected bilaterally into dorsal hippocampal CA1 region of *Pvalb-cre* (PV-Cre) transgenic mice[32] (aged between postnatal days 15–19) at three sites: 2.2, 1.8 and 1.6 mm posterior from bregma, 2.4, 2.1, 1.7 mm from midline, and 1.2, 1.1, and 1 mm below cortical surface, respectively. Animals were anesthetized with isoflurane, mounted in a stereotactic apparatus and kept under isoflurane anesthesia during

surgery. We injected 100 nL of virus at each location over a 2 min period using a glass micropipette (tip diameter ~20 μm) attached to a Nanoliter 2000 pressure injection apparatus (World Precision Instruments). The pipette was held in place for 3 min following each injection before being completely retracted from the brain. Mice were returned to their home cage for 2–3 weeks before acute slice preparation to allow for virus expression.

Computational model of EPSP-spike coupling

The computater modeling was performed using NEURON and automated using MATLAB. A simplified pyramidal cell, consisting of a soma, a single axon and a single dendrite was initialized to starting parameters before each stimulus. Background and voltage-gated conductances were based on reported models[33,34]. Small adjustments were made to improve agreement of parameters such as cell excitability and action potential waveform between the model and experimental observations. Each sweep consisted of (1) a "monosynaptic" EPSC onto the dendrite, (2) a "disyanptic" feed-forward IPSC onto the soma and dendrite 2 ms after the evoked EPSC (unless otherwise specified), and (3) multiple "spontaneous" IPSCs onto the soma with randomly distributed amplitudes and timing. To isolate the role of the feed-forward IPSC from changes in inhibitory-tone, spontaneous IPSCs were omitted in the simulation used to generate Fig 4h,i. At the outset of each set of sweeps, the "evoked" EPSC-IPSC amplitudes were set empirically by increasing the EPSC and IPSC conductances together with a fixed ratio of 6:1 until ~50% chance of spike propagation was reached. Experimental measurement of IPSC/EPSC ratio ranged from 2.62 to 5.20 (mean ±S.E.M. of 3.65±0.28). This experimentally measured range is presumed to be an underestimate of the true ratio due to imperfect isolation of the IPSC reversal potential, causing a presumed GABAergic contribution to the measured EPSC in some cells. In the model, IPSC/EPSC ratios from 4:1 up to 6:1 showed a pronounced TGOT-induced increase in evoked spike probability, with 6:1 supporting the strongest influence of TGOT on spike timing and jitter. Variability was introduced by using pseudo-random number generation to vary independently (1) the evoked EPSC conductance, (2) the evoked IPSC conductance and (3) the spontaneous IPSC timing and amplitudes. Evoked EPSC and IPSC conductances were varied independently on each sweep according to a normal distribution centered on the empirically determined mean value, with a standard deviation that was 5% of the mean. TGOT was simulated by (1) reducing the evoked somatic IPSC conductance to 60% of "baseline", while sparing the evoked EPSC and the dendritic IPSC, (2) doubling the spontaneous IPSC amplitude, and (3) increasing the spontaneous IPSC rate from 5 Hz to 35 Hz. The IPSC reversal potential was set at −110 mV for Fig S10b–c, consistent with the calculated $GABA_A$ reversal potential in our whole cell recording conditions. For the rest of the simulations, the IPSC reversal potential was set to −90 mV, consistent with cell-attached recording conditions. The increase in evoked spike probability was robust as the $GABA_A$ reversal potential was varied from −80 mV to −120 mV (Fig S12), while the reduction in latency and latency jitter were decreased in magnitude but remained statistically significant.

Supplementary Material

Refer to Web version on PubMed Central for supplementary material.

Acknowledgements

References

1. Domes G, Heinrichs M, Michel A, Berger C, Herpertz SC. Oxytocin improves "mind-reading" in humans. Biol Psychiatry. 2007; 61:731–733. [PubMed: 17137561]

2. Ferguson JN, Aldag JM, Insel TR, Young LJ. Oxytocin in the medial amygdala is essential for social recognition in the mouse. J Neurosci. 2001; 21:8278–8285. [PubMed: 11588199]

3. Tomizawa K, et al. Oxytocin improves long-lasting spatial memory during motherhood through MAP kinase cascade. Nat Neurosci. 2003; 6:384–390. [PubMed: 12598900]

4. Knobloch HS, et al. Evoked axonal oxytocin release in the central amygdala attenuates fear response. Neuron. 2012; 73:553–566. [PubMed: 22325206]

5. Modahl C, et al. Plasma oxytocin levels in autistic children. Biol Psychiatry. 1998; 43:270–277. [PubMed: 9513736]

6. Wu S, et al. Positive association of the oxytocin receptor gene (OXTR) with autism in the Chinese Han population. Biol Psychiatry. 2005; 58:74–77. [PubMed: 15992526]

7. Muhlethaler M, Charpak S, Dreifuss JJ. Contrasting effects of neurohypophysial peptides on pyramidal and non-pyramidal neurones in the rat hippocampus. Brain Res. 1984; 308:97–107. [PubMed: 6478205]

8. Pouille F, Scanziani M. Enforcement of temporal fidelity in pyramidal cells by somatic feed-forward inhibition. Science. 2001; 293:1159–1163. [PubMed: 11498596]

9. Buzsaki G, Eidelberg E. Commissural projection to the dentate gyrus of the rat: evidence for feed-forward inhibition. Brain Res. 1981; 230:346–350. [PubMed: 7317783]

10. Zaninetti M, Raggenbass M. Oxytocin receptor agonists enhance inhibitory synaptic transmission in the rat hippocampus by activating interneurons in stratum pyramidale. Eur J Neurosci. 2000; 12:3975–3984. [PubMed: 11069593]

11. Foldy C, Lee SY, Szabadics J, Neu A, Soltesz I. Cell type-specific gating of perisomatic inhibition by cholecystokinin. Nat Neurosci. 2007; 10:1128–1130. [PubMed: 17676058]

12. Wilson RI, Kunos G, Nicoll RA. Presynaptic specificity of endocannabinoid signaling in the hippocampus. Neuron. 2001; 31:453–462. [PubMed: 11516401]

13. Yoshida M, et al. Evidence that oxytocin exerts anxiolytic effects via oxytocin receptor expressed in serotonergic neurons in mice. J Neurosci. 2009; 29:2259–2271. [PubMed: 19228979]

14. Alberi S, Dreifuss JJ, Raggenbass M. The oxytocin-induced inward current in vagal neurons of the rat is mediated by G protein activation but not by an increase in the intracellular calcium concentration. Eur J Neurosci. 1997; 9:2605–2612. [PubMed: 9517466]

15. Galarreta M, Hestrin S. Frequency-dependent synaptic depression and the balance of excitation and inhibition in the neocortex. Nat Neurosci. 1998; 1:587–594. [PubMed: 10196566]

16. Kraushaar U, Jonas P. Efficacy and stability of quantal GABA release at a hippocampal interneuron-principal neuron synapse. J Neurosci. 2000; 20:5594–5607. [PubMed: 10908596]

17. Persico AM, Bourgeron T. Searching for ways out of the autism maze: genetic, epigenetic and environmental clues. Trends Neurosci. 2006; 29:349–358. [PubMed: 16808981]

18. Guastella AJ, et al. Intranasal oxytocin improves emotion recognition for youth with autism spectrum disorders. Biol Psychiatry. 2010; 67:692–694. [PubMed: 19897177]

19. Anagnostou E, et al. Intranasal oxytocin versus placebo in the treatment of adults with autism spectrum disorders: a randomized controlled trial. Molecular autism. 2012; 3:16. [PubMed: 23216716]

20. Gogolla N, et al. Common circuit defect of excitatory-inhibitory balance in mouse models of autism. J Neurodev Disord. 2009; 1:172–181. [PubMed: 20664807]

21. Dinstein I, et al. Unreliable evoked responses in autism. Neuron. 2012; 75:981–991. [PubMed: 22998867]

22. Kinsley CH, et al. Motherhood improves learning and memory. Nature. 1999; 402:137–138. [PubMed: 10647003]

23. Verret L, et al. Inhibitory interneuron deficit links altered network activity and cognitive dysfunction in Alzheimer model. Cell. 2012; 149:708–721. [PubMed: 22541439]

24. Lee SH, et al. Activation of specific interneurons improves V1 feature selectivity and visual perception. Nature. 2012; 488:379–383. [PubMed: 22878719]

25. Glickfeld LL, Scanziani M. Distinct timing in the activity of cannabinoid-sensitive and cannabinoid-insensitive basket cells. Nat Neurosci. 2006; 9:807–815. [PubMed: 16648849]

26. Madison DV, Nicoll RA. Actions of noradrenaline recorded intracellularly in rat hippocampal CA1 pyramidal neurones, in vitro. J Physiol. 1986; 372:221–244. [PubMed: 2873241]

27. Segal M, Bloom FE. The action of norepinephrine in the rat hippocampus. IV. The effects of locus coeruleus stimulation on evoked hippocampal unit activity. Brain Res. 1976; 107:513–525. [PubMed: 178411]

28. Kuo SP, Trussell LO. Spontaneous spiking and synaptic depression underlie noradrenergic control of feed-forward inhibition. Neuron. 2011; 71:306–318. [PubMed: 21791289]

29. Bergles DE, Doze VA, Madison DV, Smith SJ. Excitatory actions of norepinephrine on multiple classes of hippocampal CA1 interneurons. J Neurosci. 1996; 16:572–585. [PubMed: 8551341]

30. Doze VA, Cohen GA, Madison DV. Synaptic localization of adrenergic disinhibition in the rat hippocampus. Neuron. 1991; 6:889–900. [PubMed: 1675862]

Supplementary References

31. Freund TF, Buzsaki G. Interneurons of the hippocampus. Hippocampus. 1996; 6:347–470. [PubMed: 8915675]

32. Hippenmeyer S, et al. A developmental switch in the response of DRG neurons to ETS transcription factor signaling. PLoS Biol. 2005; 3:e159. [PubMed: 15836427]

33. Ascoli GA, Gasparini S, Medinilla V, Migliore M. Local control of postinhibitory rebound spiking in CA1 pyramidal neuron dendrites. J Neurosci. 2010; 30:6434–6442. [PubMed: 20445069]

34. Hao J, Wang XD, Dan Y, Poo MM, Zhang XH. An arithmetic rule for spatial summation of excitatory and inhibitory inputs in pyramidal neurons. Proc Natl Acad Sci U S A. 2009; 106:21906–21911. [PubMed: 19955407]

35. Shu Y, Hasenstaub A, Duque A, Yu Y, McCormick DA. Modulation of intracortical synaptic potentials by presynaptic somatic membrane potential. Nature. 2006; 441:761–765. [PubMed: 16625207]

36. Atallah BV, Scanziani M. Instantaneous modulation of gamma oscillation frequency by balancing excitation with inhibition. Neuron. 2009; 62:566–577. [PubMed: 19477157]
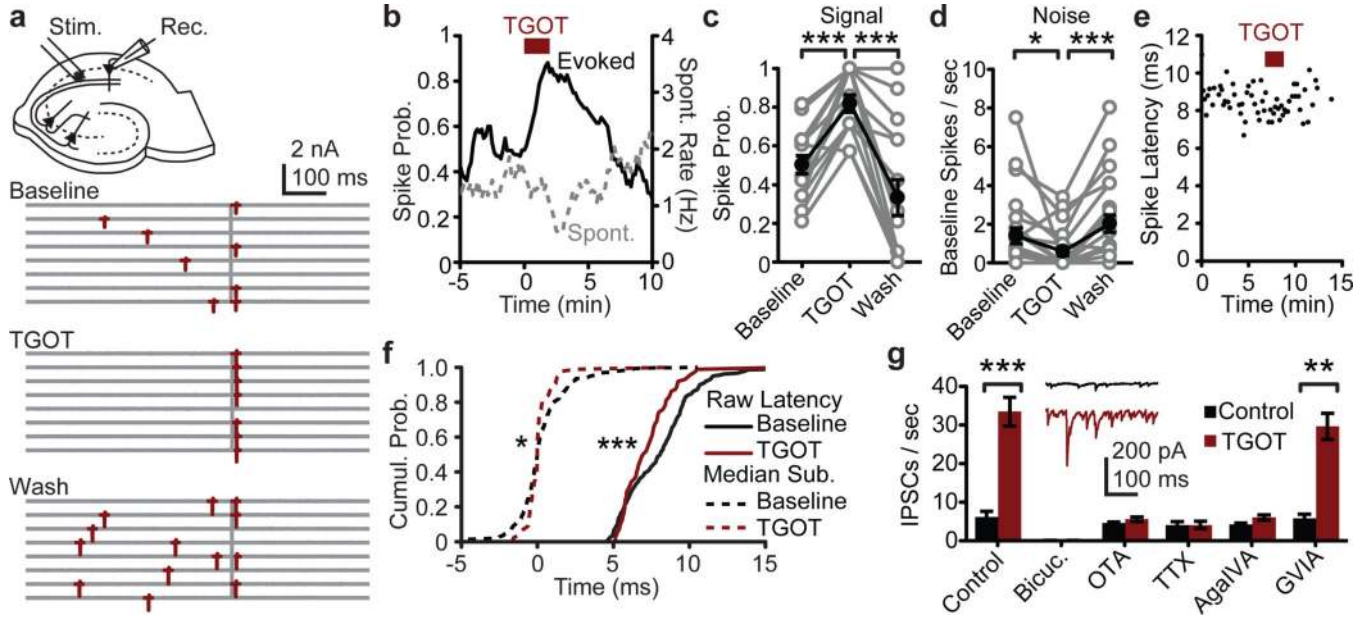
Figure 1. Oxytocin receptor agonist (TGOT) reduces spontaneous firing but enhances EPSP-spike coupling in CA1 pyramidal neurons

a, Exemplar CA1 pyramidal cell-attached recording. Vertical bar indicates SC stimulus. **b**, Time course and **c,d**, Group data of evoked spike probability (N=15 cells) and spontaneous activity (N=23 cells) in pyramidal cell-attached recordings as influenced by 200 nM TGOT. **e**, Exemplar recording demonstrating TGOT reduction in evoked spike latency and jitter. **f**, Cumulative distribution of raw (solid) and mean-subtracted (dashed) spike times (N=15 cells). Mean latency: 5.87±0.42 ms; Mean variance: 2.29±0.30 ms^2. **g**, Spontaneous IPSC frequency onto CA1 pyramidal cells (N=6 cells, each condition). Paired two-tailed *t*-test in panels c,d,g. Two-sample K-S test in panel f. *, P<0.05; **, P<0.01; ***, P<0.001. Error bars, S.E.M.
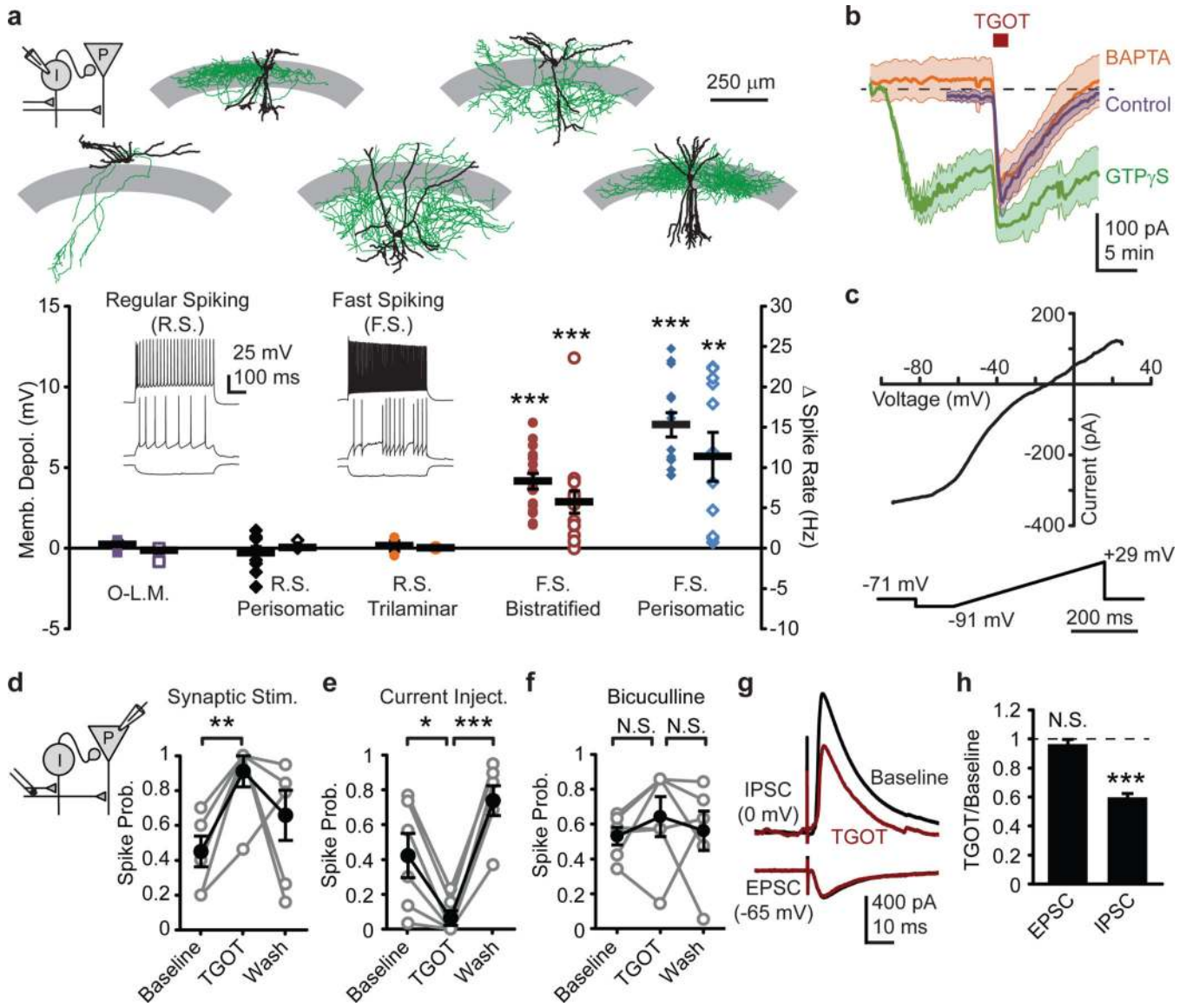
Figure 2. TGOT activates FSIs and suppresses feed-forward inhibition

a, TGOT influence on membrane potential (filled symbols) and firing rate (open symbols). Exemplar electrophysiological identification of interneurons, inset. Above, exemplar biocytin-filled interneurons tracings (soma and dendrites, black; axon, green; stratum pyramidale, gray area). O-LM (N=3), RS basket (N=9), RS trilaminar (N=3), FS bistratified (N=16), and FS perisomatic-targeting (N=14). **b**, Voltage clamp recordings of average TGOT currents ±S.E.M (shaded) in FSIs with control, 10 mM BAPTA, and 1 mM GTPγS filled pipettes (N=7, each condition). **c**, Voltage-dependence of TGOT-induced current in exemplar FSI. **d,e**, Whole cell spike probability from synaptically (panel d) or current injection-evoked spikes (panel e) in the same set of pyramidal neurons (N=6 cells). **f**, Cell-attached, synaptically-evoked spike probability in bicuculline (N=6 cells, Probability: P>0.95; Latency: P>0.5; Latency variance: P>0.3). Reduced stimulus strength was sufficient to reach 50% spike transmission and spikes occurred at longer latencies and with more jitter

than in control ACSF[8]. **g**, TGOT influence on average evoked disynaptic IPSC from one pyramidal cell and monosynaptic EPSC from a different pyramidal cell. **h**, Normalized group data for evoked EPSC (N=6 cells) and disynaptic IPSC (N=8 cells). Paired two-tailed *t*-test, all panels except panel d, which uses one-tailed *t*-test for compatibility with cell-attached results. *, P<0.05, **, P<0.01; ***, P<0.001. Error bars S.E.M.
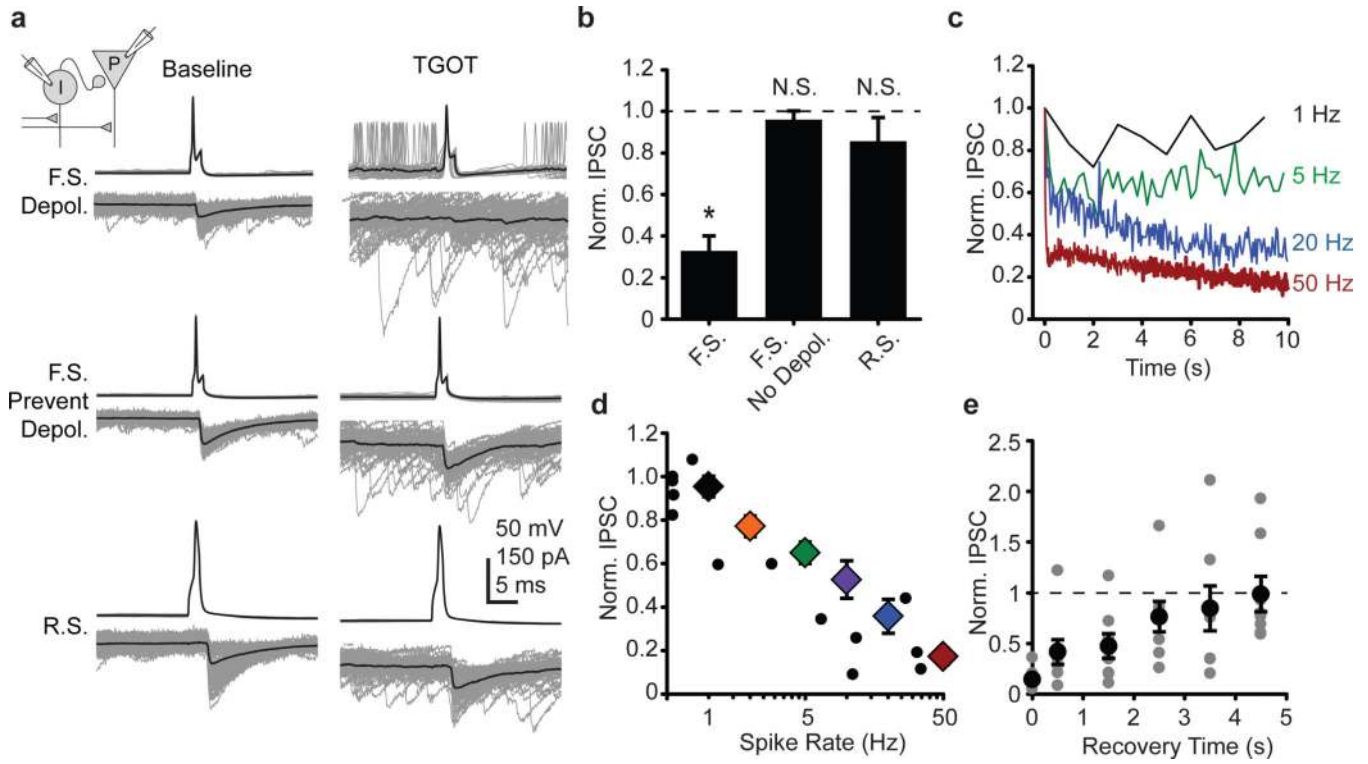
Figure 3. Paired recordings reveal synaptic locus of TGOT-induced decrease in evoked inhibition
a, Presynaptic interneuron (upper) and postsynaptic pyramidal cells (lower). Individual
sweeps in gray, average in black. Top: presynaptic FSI permitted to depolarize in TGOT.
Middle: TGOT depolarization of presynaptic FSI countered by current injection. Bottom: RS
interneuron transmission unaffected by TGOT. **b**, FSI-pyramidal synapses depress only
when FSI is depolarized by TGOT. FSI, N=8; No depolarization, N=5; RS, N=4. **c**,
Frequency-dependent depression of FSI-pyramidal cell synapses in control ACSF. Averages
normalized to first IPSC. **d**, FSI-pyramidal synaptic depression from TGOT-induced firing
(black circles, one point per cell pair) matches depression by 10 s spike trains in control
ACSF (colored diamonds, average from multiple cell pairs). No black circles obscured by
colored diamonds. **e**, Synaptic recovery following 50 Hz, 10 s train. (N=8 cells). Paired two-
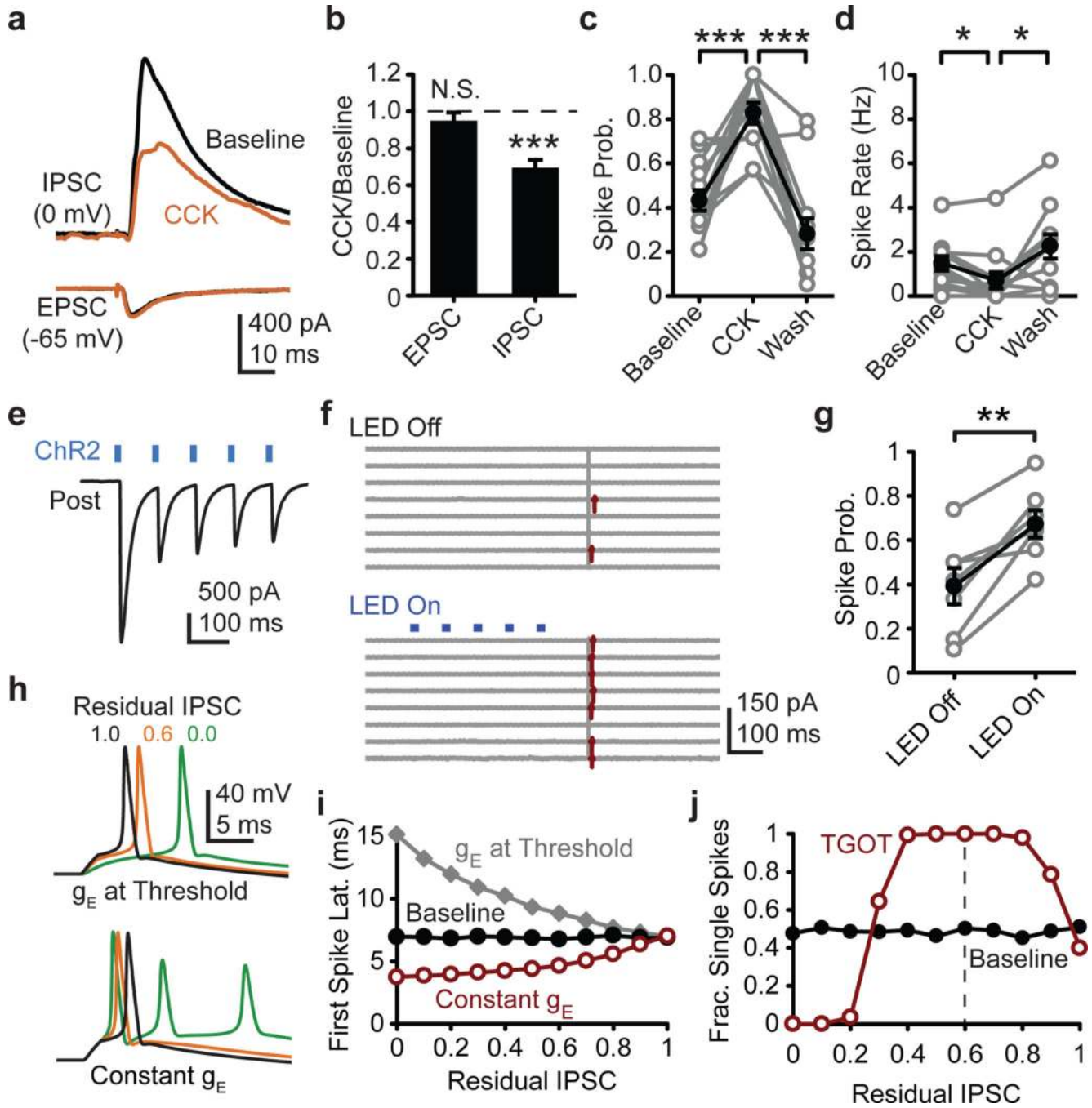tailed *t*-test. *, P<0.05. N.S. P>0.15. Error bars S.E.M.

Figure 4. Generalization to other brain states and modulators

a, CCK (200 nM) influence on average evoked disynaptic IPSC from one pyramidal cell and monosynaptic EPSC from a different pyramidal cell. **b**, Normalized group data for evoked EPSC (N=6 cells) and disynaptic IPSC (N=6 cells). **c**, Evoked spike probability (N=14 cells) and **d**, spontaneous firing rate (N=14 cells) in cell-attached recordings as influenced by CCK. **e**, Exemplar ChR2-evoked IPSCs recorded in a CA1 pyramidal neuron from a PV-cre mouse injected with double-floxed AAV-ChR2. **f**, Cell-attached recording from mouse CA1 pyramidal neuron. Control (LED off) and ChR2 stimulation (LED on) sweeps interleaved

during recording, but grouped for presentation. **g**, ChR2 influence on cell-attached spike probability in the subset of mouse pyramidal neurons in which latency and jitter indicated a minimal monosynaptic inhibition (see methods). **h**, Computer simulated exemplar traces in which IPSC conductance (g_{IPSC}) is reduced and EPSC conductance (g_{EPSC}) is either lowered to maintain ~50% chance of spiking (top) or g_{EPSC} is held constant (bottom). **i**, Residual IPSC influence on simulated spike latency with g_{EPSC} held constant (red) or reduced to maintain ~50% spike probability (gray). Panels h and i generated in absence of spontaneous IPSCs to isolate feed-forward IPSC contribution to evoked spike timing. **j**, Residual IPSC influence on probability of eliciting exactly one spike (g_{EPSC} held constant). Paired two-tailed *t*-test. *, P<0.05; **, P<0.01; ***, P<0.001. Error bars S.E.M.